Iris Recognition System Evaluation Experiments Using CASIA Version3

Samar Al-Saqqa[1], Mohammad Al-Rawi[2], Moh'd Belal Al- Zoubi[3]

[1.]Department of Business Information Technology, King Abdullah II School for Information Technology, The University of Jordan, Amman 11942 Jordan
[2.]Department of Computer Science, King Abdullah II School for Information Technology, The University of Jordan, Amman 11942 Jordan
[3.]Department of Computer Information Systems, King Abdullah II School for Information Technology, The University of Jordan, Amman 11942 Jordan
s.alsaqqa@ju.edu.jo

Abstract: In this paper, we provide new evaluation experiments on iris recognition system, these experiments are based on different evaluation metrics which investigate the iris recognition system accuracy using a new version of the well-known public database CASIA version3. Two datasets from CASIA V3-Interval database are used, the first set is set100 contains 100 images and the second set is set2421 contains 2421 images, to get the best recognition the optimum values of the 1-D log Gabor filter parameters are recorded to each set. The registered False Accept Rate (FAR) and False Reject Rate (FRR) using Set2421 are 0.07%, 0.12% respectively when the separation threshold value is 0.4, while FAR and FRR are zeros using Set100 when the separation threshold value is 0.39. The relation between FAR and FRR for different values of the threshold is represented by Receiver Operating Curve (ROC). The recommended template size to use is [20x200] and the number of shifts is eight.
[Samar Al-Saqqa ,Mohammad Al-Rawi, Moh'd Belal Al- Zoubi. **Iris Recognition System Evaluation Experiments Using CASIA Version3**. *J Am Sci* 2013;9(9):117-127] (ISSN: 1545-1003) http://www.jofamericanscience.org. 17

1. Introduction

Iris recognition is based on recognizing and identifying people by analyzing their iris patterns. It is considered an accurate, secure and reliable biometric technique (Daugman, 1993; Wildes, 1997; Jain et al., 1999; Saba et al., 2013; Mansfield and Wayman, 2002; Daugman, 2003; Saba and Rehman, 2013), it has advantages due to the iris complex patterns, the stability of the iris pattern after one year, its difficulty to be imitated and faked, and its simplicity to capture and encode (Rahim et al., 2012). The iris is the annular area between the pupil and the white sclera in the eye. It has a rich texture based on interlacing features that are called the texture of the iris. This texture is well-known to provide a signature that is unique to each subject. (Daugman, 1993; Saba and Altameem; 2013).

A typical iris recognition system consists of four phases: Image acquisition, Iris localization (detecting the iris inner and outer boundaries), Normalization, Feature extraction and matching patterns. Image Acquisition is the first phase of the iris recognition system which includes capturing a sequence of iris images from the person using specifically designed sensor or light-sensitive cameras. The second phase is iris localization which is the process of locating and detecting the iris inner and outer boundaries (pupil and sclera). The third phase is normalization, the main purpose of the normalization

phase is to recognize the irises regardless of the size, position and rotation, and eliminate dimensional inconsistencies between irises. Encoding is the fourth phase which is the automated process of extracting the distinctive information in iris patterns in order to generate and build templates so that comparisons between the templates can be done. Template matching is the last phase in the iris recognition system, it measures the similarity between two iris patterns and gives the result to identify or deny the person. Figure 1 shows the different phases of iris recognition system.
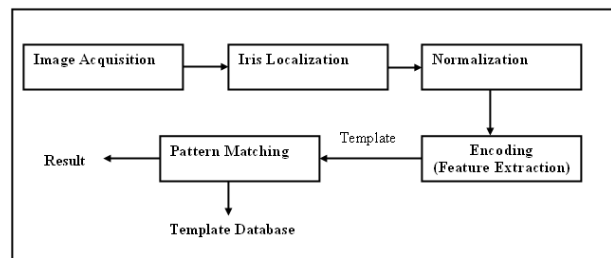
Figure 1. The typical iris recognition system

The first complete iris recognition system was designed and patented by J.Daugman (Daugman, 1993). It was followed by a number of other works in the field of iris recognition. Many of these methods focus on proposing a new method, or optimizing for specific stages in the iris recognition.

In this research, we focus on evaluation and performance analysis for iris recognition methods and algorithms, we depend on evaluation model that has important metrics to evaluate the system. These metrics include: The False Accept Rate (FAR), the False Reject Rate (FRR), and the Receiver Operating Curve (ROC), which represents the relation between the FAR and FRR for different values of thresholds that are used to show the performance. The decidability is also used to indicate how much the imposters and genuine are separate. We found the optimal values of the Gabor filter parameters and other system parameters that give the best performance of the iris recognition system, the obtained statistics show the effect of changing the filter parameters values on the decidability.

In our experiments and evaluation we used the open source code for biometric identification system based on the iris patterns implemented by Masek and Kovesi (Masek, 2003). This software is publicly available for research and evaluation purposes, but since the system was implemented by the MATLAB software package, we re-implemented the most computation intensive stages in this system in C++ to improve the speed of the system. Masek used CASIA Iris Image Database version1.0 (CASIA-IrisV1), publicly provided by Chinese Academy of Sciences - Institute of Automation, to evaluate the iris recognition system. We used the new version of CASIA that is version3.0 (CASIA-IrisV3).

## 2. Implementation of Iris Recognition System stages

2.1 CASIA Database

CASIA V3 is the latest version of CASIA databases (2006). It contains a total of 22,051 iris images from more than 700 subjects. The images are divided into the following three data sets: CASIA-IrisV3-Interval, CASIA-IrisV3-Lamp and CASIA-IrisV3-Twins. The data sets were collected in different times. All iris images are 8 bit gray-level. CASIA V3 images compared to CASIA V1 are Original unmasked images and now the CASIA V1 is not recommended to use (Jonathon et al., 2007). Figures 2 and 3 show examples of the images in each database.

We used one data set from CASIA, which is the CASIA-IrisV3-Interval dataset because it is almost better than CASIA-IrisV3-Lamp and CASIA-IrisV3-Twins. CASIA-IrisV3-Interval includes 2655 images from 249 subjects with a 320x280 resolution. Most images were captured in two sessions with at least one month interval.

2.2 Segmentation

Hough transform is used for detecting the outer and inner boundaries, which are the iris/sclera boundary and iris/ pupil boundaries. This process will be preceded by using the Canny's edge detection to generate the edge map image. Only the strongest edges will be detected by controlling the parameters of Canny's edges detector, (e.g. sigma which is the standard deviation of Gaussian smoothing filter, the weighting for vertical and horizontal gradients, lower and upper radius of the iris and pupil to search for, and the threshold for connected edges). The range of iris and pupil radii was set manually. For CASIA V3 images, we chose to use 85 to 155 pixels as the iris radius range, while the pupil radius range is from 25 to 75 pixels.
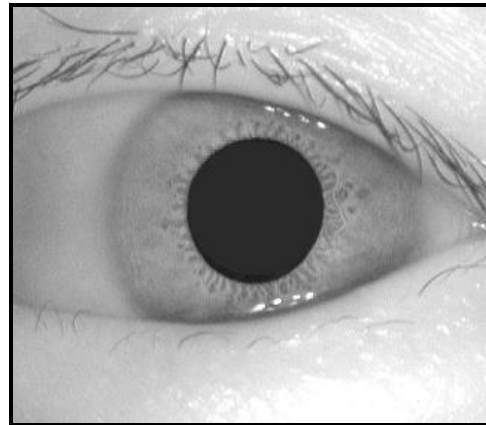
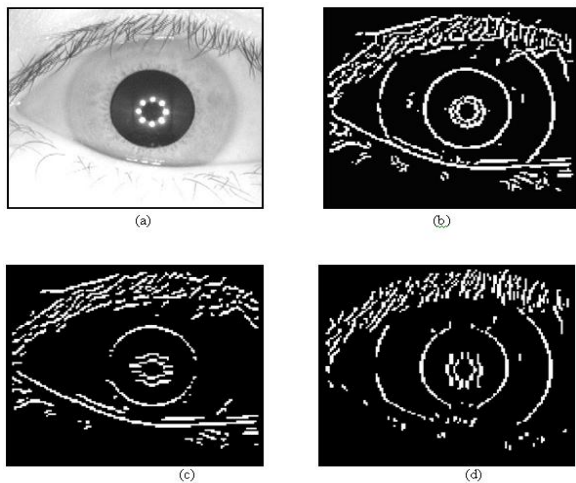**Figure 2.** An image from CASIAV1.
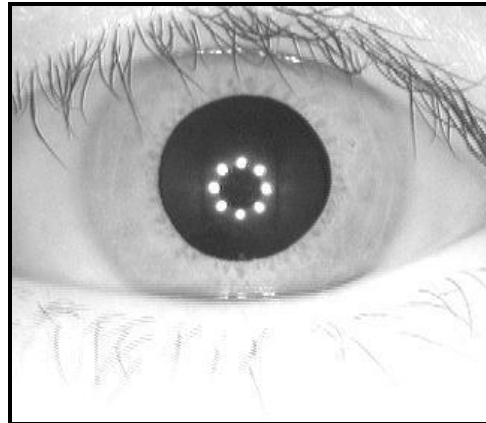
**Figure 3.** An image from CASIA-IrisV3-Interval.

To detect the outer iris boundary, the vertical gradient is used as suggested by (Wildes, 1997). This will reduce the influence of the eyelid edge map on the outer iris boundary edge map, taking into consideration the horizontal alignment of the eyelids as shown in figure 4. The inner boundary of the iris, iris /pupil boundary, was detected by setting the horizontal and vertical gradients of the Canny edge

detector to be equal, then the circular Hough transform is used. Eyelids were detected by using the horizontal gradient of the Canny edge detection to generate the edge map followed by using the linear Hough transform. The eyelashes were isolated by simple thresholding.

We have got a success rate in the segmentation of around 91.2% (2421 out of 2655). Some images failed in the segmentation due to their poor quality. Figure 5 shows some examples of images after the segmentation stage and figure 6 shows some examples of images segmentation errors.


Figure 4. Canny's edge detection applying on an image using the vertical and horizontal gradients. (a) Original image from CASIA V3. (b) Corresponding edge map, the vertical and horizontal gradients were weighted equally. (c) Corresponding edge map with horizontal gradient. (d) Corresponding edge map with vertical gradient.
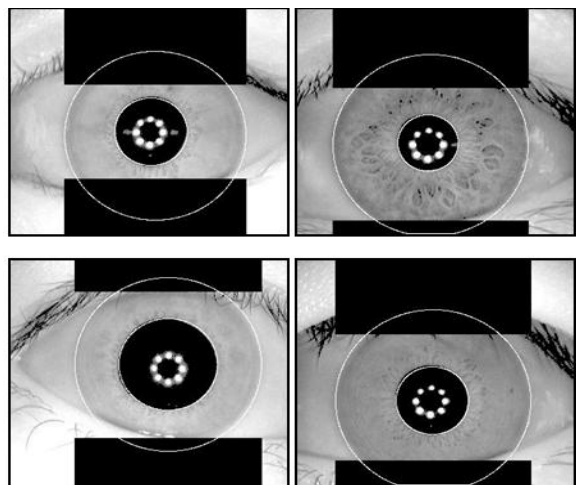
Figure 5. Examples of images after the segmentation stage.
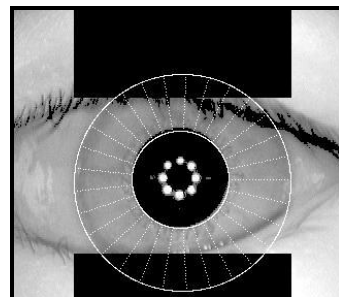
2.3 Normalization

The next stage after the successful segmentation is mapping the iris region (annular region) to a rectangular one which has a fixed dimension without any dimensional inconsistencies such as the size of the iris in the image, the size of the pupil in the image, and the iris orientation. Masek used Daugman's Rubber Sheet model for the iris normalization. The homogenous rubber sheet model proposed by Daugman (Daugman,1993) remaps each point within the iris region to a pair of dimensionless non-concentric polar coordinates (r,θ) where r is on the interval $[0,1]$ and θ is an angle $[0,2\pi]$.
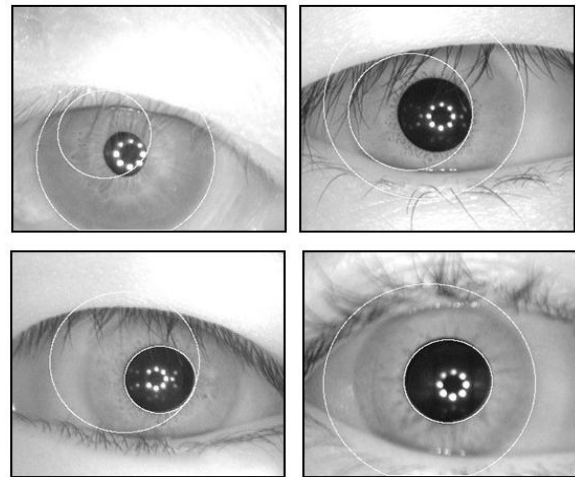
Figure 6. Examples of wrong segmentations

We set manually two parameters, the angular resolution, which is the number of radial lines going along the iris region, and the radial resolution, which is the number of iris points sampled along each radial line. As shown in figure 7.

The normalization process produces two two-dimensional arrays (2D array) with horizontal and vertical dimensions corresponding to the angular and the radial resolution, and the second one is created to mark regions that contain reflections or that are occluded by eyelids and eyelashes. We obtained almost successful results of the normalization stage. Figures 7 show the normalization process.

Figure 7. The normalization process with radial resolution of 20 pixels, and the angular resolution of 30 pixels.

2.4 Feature Encoding

1-D Log-Gabor filters were chosen by Masek (Masek,2003) to be the feature extractor. By applying 1-D Log-Gabor Filters, a 2D normalized iris pattern is first decomposed into a number of 1-D signals, and these 1-D signals are convolved with 1-D Log-Gabor wavelets then the output of convolution is phase quantized to four levels using Daugman method (Daugman, 2003). Each pixel in the normalized iris pattern corresponds to two bits of data in the iris template and this operation is repeated all across the iris. The output of the encoding stage is the template which contains a number of bits of feature information and the corresponding noise mask which corresponds to invalid and corrupted iris regions and marks the bits in template also as corrupt. (Figure 8).

Figure 8. The iris template (Iris Code) resulted from the encoding

2.5 Template Matching

The Hamming Distance (HD) that is proposed by Daugman (Daugman, 1993), (Daugman, 2004) was applied as a metric for iris matching. The two 2D arrays were used, the first array is the template that contains the information bits, and the second is the noise mask that contains the non-valid bits. The HD calculation was done by counting the different bits of two templates in the iris regions where both the noise masks had zeros values. The HD for the two templates X and Y is given as follows:

$$HD(X,Y) = \frac{\sum_{i=1}^{N}(X_i(XOR)Y_i(AND)ValidBits_i)}{\sum_{i=1}^{N}ValidBits_i}$$

Where

$$ValidBits_i = \begin{cases} 1 \text{ if } X_i \text{ noise mask=0 and } Y_i \text{ noise mask=0;} \\ 0 \quad \text{otherwise} \end{cases}$$

3. Iris Recognition System Evaluation metrics

Many performance metrics are used to evaluate the iris recognition system as shown in figure 9, we depend on the following criteria in the iris recognition system evaluation:

1-Hamming Distance: the Hamming Distance (HD) is used as a matching metric. The HD is calculated by counting non-matching bits of two templates where both masks had zeros. A number of shifts are needed

to account the iris rotations, one of templates is shifted left and right to find the best match and the minimum HD is chosen and considered as a resulted HD.

2-Inter-Class and Intra-Class distributions: after the calculation of the hamming distances of all templates comparisons, the HD's file of the all comparisons will be ready, and can be analyzed to find the Intra-Class and the Inter-Class distribution. The Inter-Class distribution of the hamming distances is generated by comparing between the different irises. Intra-Class distribution is generated by comparing between different templates of the same iris.

3-Decidability: to test the separability of the iris recognition system, the decidability measure proposed by Daugman (Daugman, 1993) is used. The decidability differentiates the Inter-Class from the Intra-Class. The higher the decidability is, the less error is found when differentiating between two distributions of the inter-class and the intra-class. The mean and the standard deviation of intra-class and inter-class distributions are calculated in order to calculate the decidability.

The decidability is represented as follows:

$$d' = \frac{|u_S - u_D|}{\sqrt{\frac{(\sigma_S^2 + \sigma_D^2)}{2}}}$$

Where u_S is the mean of the intra-class distribution, u_D is the mean of the inter-class distribution, σ_D is the standard deviation of the inter-class distribution and σ_S is the standard deviation of the intra-class distribution.

4-Degree Of Freedom (DOF): the uniqueness of the iris patterns means that there is an independent variation in the iris detail (Daugman, 1993); we can determine the iris uniqueness by examining the Inter-Class distribution resulting from comparing between the different templates, which are generated from different irises. Uniqueness can be determined by calculating the degree of freedom for the hamming distance distribution obtained from comparing between templates of different irises. The degree of freedom is calculated as follows:

$$DOF = \frac{p(1-p)}{\sigma^2}$$

Where the p is the mean and σ is the standard deviation of inter-class distribution.

5-False Reject Rate (FRR) and False Accept Rate (FAR): At each Hamming distance Criteria (HDC) (or Threshold), the hamming distance resulted from comparing between two images is compared with

HDC if it is equal or above or below HDC. If the two images are similar and the hamming distance is above HDC then false reject case is happened and False Reject count (FRC) will added by one. If the two images are different and the hamming distance is below HDC then the False Accept Count (FAC) will be added by one. The FRC is divided by the total number of intra class comparisons to find the FRR, while the FAC is divided by the total number of inter-class comparisons to find FAR, the perfect iris recognition system is the system in which its error rates FAR and FRR are zeros.

6-Receiver Operating Curve (ROC) It is a graphical depiction of the relationship between the FRR and FAR as a function of the threshold's value. If the plot lies closer to the axis then the performance of the iris recognition system will be better.
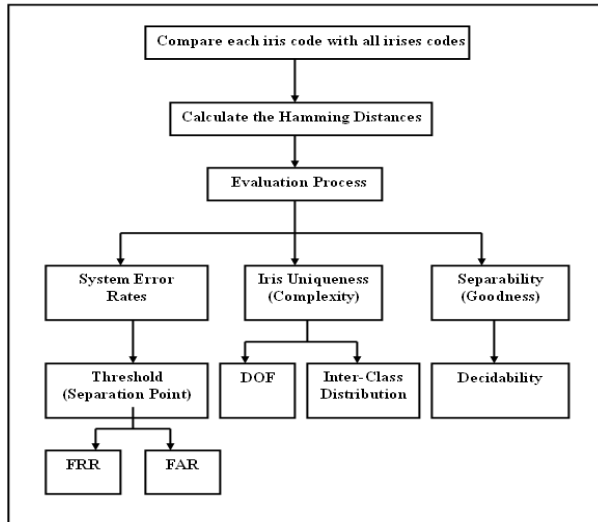
Figure 9. Block diagram illustrates the evaluation process using different evaluation metrics based on liber masek experiments method

4. Optimization of Iris Recognition System

In this work, many experiments are done in order to improve the iris recognition system performance. These experiments are based on making an optimization for the iris recognition system to find the best parameters. Many parameters play an important role in increasing or decreasing the performance of the iris recognition system. These parameters are:

1-LOG Gabor filter Parameters: such as the number of filters to use (Nscales), the wavelength of the basis filter (Wavelength), the multiplicative factor between each filter (Mult), and ratio of the standard deviation of the Gaussian describing the log gabor filter's transfer function in the frequency domain to the filter center frequency (SigmaOnf), searching for SigmaOnf in the range [0.025,0.8] and the

increment is 0.025, Nscales in the range [1,5], Mult in the range [1,3], and searching for the Wavelength in the range [1,20]. The decidability is calculated at different values of parameters and the parameters that give the maximum decidability are considered as the best values which can be used in the system.

2-Template Size: this is defined by the radial and angular resolution. In the experiments many radial and angular resolutions are applied in order to find the best template size that achieves the good performance beside the efficient storage.

3-Number of shifts: a number of shifts are needed to account the rotational inconsistencies between any two-iris templates.

5. Evaluation and Experimental Results
### 5.1. Data Sets

Two dataset of images which are obtained from the CASIA V3-Interval database are used, Set100 and Set2421. The first dataset is subset from the second dataset and all the images it contains are chosen from Set2421. The details of these subsets and their total number of comparisons are shown in table 1.

Table 1. Iris images datasets taken from the CASIAV3-Interval and used in the testing and evaluation

| CASIA v3-Interval Testing Sets Names	Set100	Set2421
Number of Iris Images	100	2421
Number of intra-Class Comparisons	450	7756
Number of inter-Class Comparisons	4500	2921654
Total Number of Comparisons	4950	2929410

5.2 Inter-Class Hamming Distances

The distributions of the hamming distances are generated by comparing between the different irises. Templates of Set100 images and Set2421 images are shown in Figures 10 and 11.
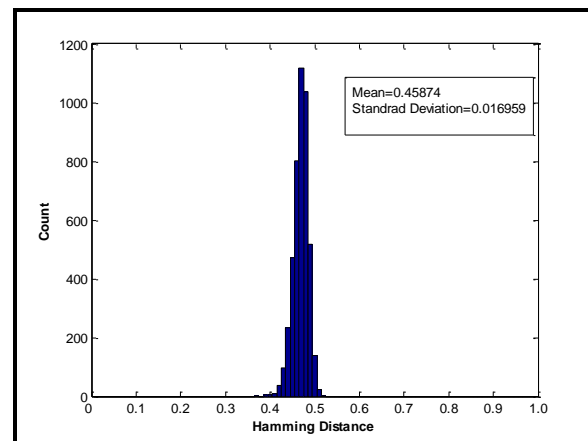
Figure 10. Inter-Class hamming distance distribution of Set100 images, encoded with template size of

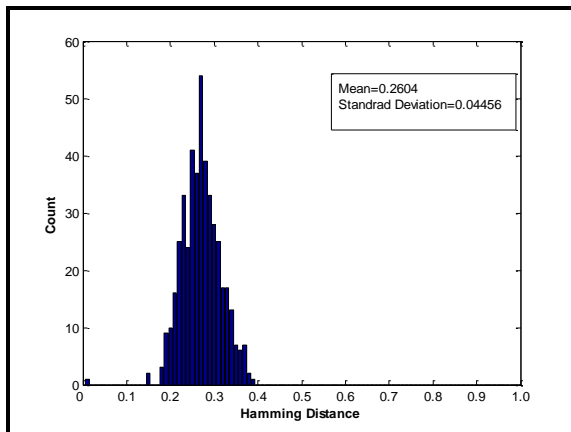[20x240]. SigmaOnf=0.5, Wavelength=16,Nscales=1 and number of shifts is 8.
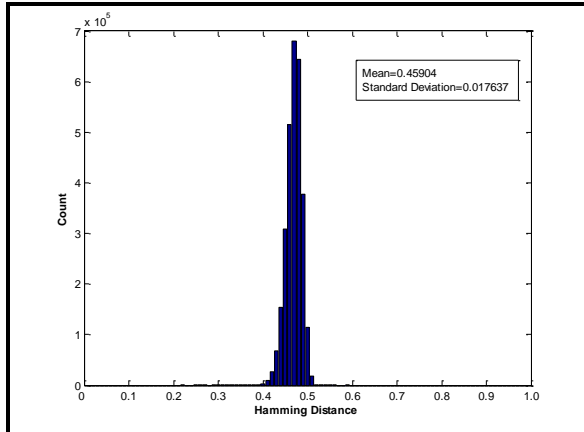
Figure 11. Inter-Class hamming distance distribution of Set2421, encoded with template size of [20x240]. Sigma On f=0.5, Wavelength=16, Nscales=1 and number of shifts is 8.

It is observed from the figure 10 and figure 11 that the mean is relatively close to 0.5, and this copes with the statistics theory, where any pair of two different irises has an equal probability of agreeing and disagreeing (Daugman, 1993).

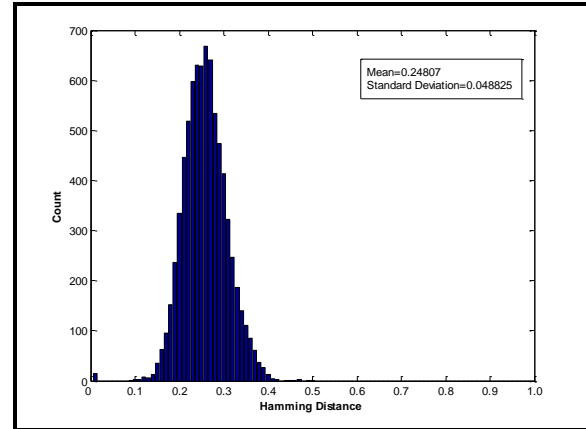**5.3 Intra-Class Hamming Distances**
The distributions of the hamming distances which are generated by comparing between different templates of the same iris are shown in figures 12 and 13.

Figure 12. Intra-Class hamming distance distribution of Set100 images, encoded with template size of [20x240].SigmaOnf=0.5, Wavelength=16, Nscales=1 and number of shifts is 8.

The hamming distances generated by comparing different images of the same iris are not zero as noticed in figures 12 and 13. This is related this

to the variations in the person angle of gaze, the degree of the eyelids and eyelashes occlusion reasons, such as light, which causes the pupil dilation (Daugman, 1993).


Figure 13. Intra-Class hamming distance distribution of Set2421 images, encoded with template size of [20x240].SigmaOnf=0.5, Wavelength=16, Nscales=1 and number of shifts is 8.

5.4 Gabor Filter parameters
The best gabor filter parameters are determined according to the maximum decidability, for the Set100 images, the highest decidability is obtained when using the centre wavelength is 12, number of filters is 1, and the filter bandwidth SigmaOnf is 0.6, while for the Set2421, the highest parameters is obtained when using the wavelength of 12 and the SigmaOnf is 0.45, and the images encoded with one filter.

The higher threshold the lower FAR, if we raise the decision threshold the FRR will be raised. Therefore the goal must to have as small FAR and FRR as possible. The distribution of the intra-class and inter-class should overlap as little as possible. Figure 14 and figure 15 show the hamming distances distributions of intra-class and the intra-class, the figure 14 shows the distribution on Set100 images while figure 15 gives the distribution using large sample of images; the Set2421 images (Elarbi-Boudihir et al., 2011).

The iris recognition system error rates, FAR and FRR, are dependent on the adjustable adopted threshold. If we increase the value of the threshold, the proportion FAR will increase, while FRR will decrease. When we decrease the value of the threshold, the proportion FAR will decrease, while FRR increases. This dependency is illustrated in table 2 and table 3. The False Reject Count (FRC) indicates the count the false rejects in the Intra-class comparisons and False Accept Count (FAC) indicates the count the false accepts in the Inter-Class comparisons.
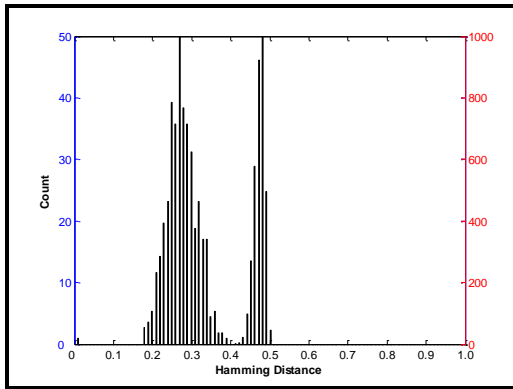
Figure 14. Intra-Class and Intra-Class distributions of Set100 using the optimal values of parameters, with [20x240] template size and 8 shifts.
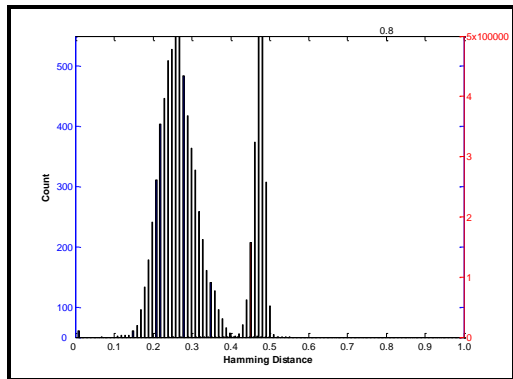
Figure 15. Intra-Class and Intra-Class distributions of Set2421 using the optimal values of parameters, with [20x240] template size and 8 shifts

Table 2. The false reject rate and the false accept rate using the Set2421 images with different hamming distance threshold (separation points) using SigmaOnf=0.45, wavelength=12, number of filters=1, and number of shifts=8.

| HD Threshold	FRC	FRR (%)	FAC	FAR (%)
0.36	146	1.88%	146	0.00%
0.37	83	1.07%	274	0.01%
0.38	40	0.52%	481	0.02%
0.39	19	0.24%	884	0.03%
0.4	9	0.12%	1943	0.07%
0.41	8	0.10%	4896	0.17%

As shown in table 2, it could take 0.4 as a separation point then FRR and FAR are 0.12% and 0.07% respectively, while if we choose the separation point 0.36 the FAR is 0% but the FRR will increase to be 1.88%

The results of best parameters and the effect of changing them on the decidability are presented below in table 4 and table 5.

Table 3. The false reject rate and the false accept rate using the Set100 images with different hamming distance threshold (separation points) using SigmaOnf=0.6, wavelength=12, number of filters=1, and number of shifts=8

HD Threshold	FRC	FRR (%)	FAC	FAR (%)
0.36	5	1.11%	0	0.00%
0.37	3	0.67%	0	0.00%
0.38	1	0.22%	0	0.00%
0.39	0	0.00%	0	0.00%
0.4	0	0.00%	0	0.00%
0.41	0	0.00%	3	0.07%

As shown in table 3, the error rates FAR and FRR will be 0% at 0.39 threshold; the separation point is clearly seen in the figure 16.
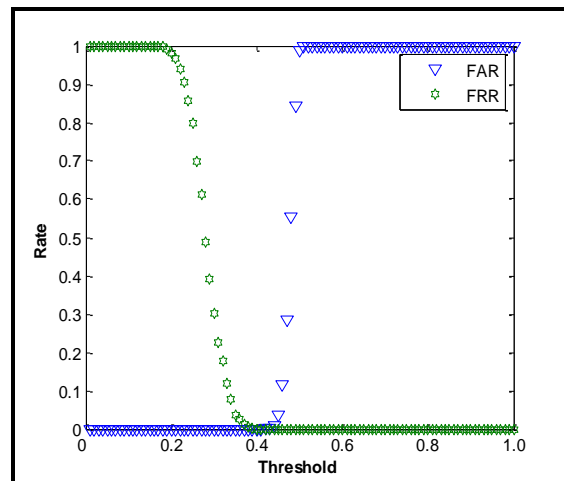
Figure 16. FRR –FAR relation using optimal values of the Gabor filter parameters on Set100, with [20x240] template size and 8 shifts.

Table 4. The decidability versus changing the filter parameters values using Set100**.**Nscales=1, template size of [20x240], and number of shifts=8.

SigmaOnf	Wavelength	u_S	u_D	σ_S	σ_D	d'
0.55	10	0.2733	0.4639	0.042	0.014	6.1678
0.55	11	0.269	0.463	0.041	0.014	6.3141
0.55	12	0.2658	0.4621	0.041	0.014	6.3463
0.55	13	0.2633	0.4614	0.042	0.014	6.3211
0.55	14	0.2621	0.4607	0.042	0.014	6.3036
0.55	15	0.2608	0.46	0.042	0.014	6.2098
0.55	16	0.2605	0.4592	0.044	0.017	6.0592
0.55	17	0.26	0.4584	0.045	0.017	5.9032
0.55	18	0.2601	0.4576	0.046	0.017	5.6811
0.6	10	0.274	0.4633	0.041	0.014	6.2209
0.6	11	0.2697	0.4626	0.041	0.014	6.3626
0.6	12	0.2657	0.4617	0.041	0.014	6.4383
0.6	13	0.2637	0.4608	0.041	0.014	6.3915
0.6	14	0.2626	0.4598	0.041	0.014	6.2995
0.6	15	0.2611	0.459	0.042	0.014	6.2559
0.6	16	0.2603	0.4582	0.042	0.017	6.1293
0.6	17	0.2602	0.4574	0.044	0.017	5.9413

Table 5. The decidability versus changing the filter parameters values using Set2421, Nscales=1, template size of [20x240], and number of shifts=8

SigmaOnf	Wavelength	u_s	u_D	σ_s	σ_D	d'
0.45	10	0.2601	0.4628	0.047	0.014	5.8878
0.45	11	0.2565	0.462	0.047	0.014	5.9355
0.45	12	0.2537	0.4612	0.047	0.014	5.9531
0.45	13	0.2513	0.4603	0.047	0.014	5.9281
0.45	14	0.2495	0.4594	0.048	0.017	5.8799
0.45	15	0.248	0.4584	0.048	0.017	5.8136
0.45	16	0.2468	0.4573	0.049	0.020	5.7185
0.45	17	0.2457	0.4561	0.049	0.020	5.6116
0.45	18	0.2448	0.4549	0.050	0.022	5.4925
0.5	10	0.2624	0.463	0.048	0.014	5.7597
0.5	11	0.2584	0.4624	0.048	0.014	5.8316
0.5	12	0.2553	0.4617	0.048	0.014	5.8685
0.5	13	0.2528	0.4611	0.048	0.014	5.8718
0.5	14	0.2507	0.4605	0.048	0.017	5.8541
0.5	15	0.2493	0.4598	0.048	0.017	5.8102
0.5	16	0.2481	0.459	0.049	0.017	5.7472
0.5	17	0.2473	0.4583	0.049	0.017	5.653

Figure 17 shows the changing of decidability when vary the Wavelength values, it is observed that the best Wavelength is 12 and the best SigmaOnf is 0.6.
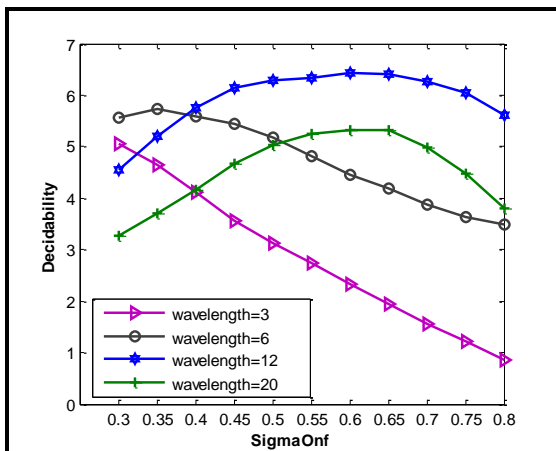

Figure 17. decidability of the Set100 images when using the different values of wavelengths and the bandwidth SigmaOnf, Nscales=1, 8 shifts and the template size of [20x240].

5.5.Receiver Operating Characteristic (ROC)

ROC curve helps to demonstrate how increasing or decreasing the threshold's value affects tradeoffs between FRR and FAR. it gives the relation between the FAR and FRR on varying the threshold. ROC curve of the iris recognition system that is used the optimal values of parameters, Wavelength=12, Nscales=1, SigmaOnf =0.45, and [20x240] as template size is shown in figure 18. The figure shows a good performance of the iris system because the ROC curve for good system can lie very near the coordinate axis. If the threshold is very low, then FAR will be almost 0 and FRR almost 1, the curve will be at a leftmost point of the ROC curve. If we increase the threshold to a middle value, the FAR will increase and FRR will decrease. Finally, as threshold is moved down to very high values, FAR will be almost 1 and FRR almost 0 and the curve will be at a rightmost point of the ROC curve.
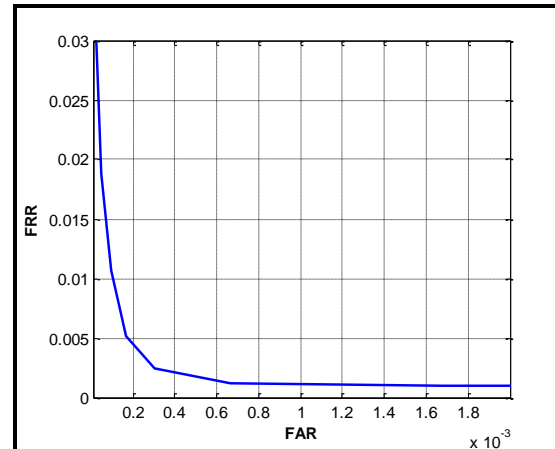
Figure 18. The ROC curve for iris recognition system using the best values of Gabor parameters, using the Set2421. Wavelength=12,Nscales=1,and the SigmaOnf=0.45, and number of shifts=8.

5.6 Uniqueness

To prove the uniqueness of the iris patterns the Degrees of Freedom (DOF) are calculated from the inter-class class distribution of Set100 and inter-class class distribution of Set2421, the DOF for the two distributions are 1338 for Set100 inter-class distribution and 1122 for Set2421 inter-class distribution. The number of degrees of freedom indicates that the differences between two irises are good.

5.7 Template Size

Different template sizes are applied on the iris recognition system in order to find the optimum template size that has a minimum size and gives relatively best decidability. The filter parameters are not fixed for searching the best template size but in contrary they are changeable with each size to obtain correct results. Not only to find the optimum size but also the optimal values of the filter parameters, the amount of the iris pattern data is determined by the radial and angular resolution used during the normalization phase. The actual template size may be calculated as angular resolution x radial resolutions x 2 x number of filters (Nscales) but it is clear the achieved performance is mostly good when the number of filters is one (Nscales=1)so the template size is calculated as angular resolution x radial

resolutions x 2. In our experiments we decided to use different values of radial and angular resolutions to find the best template size that achieves the efficiency of the identification. Table 6 presents the decidability values generated by encoding templates with various radial and angular resolutions and the optimal values of the parameters for each size.

Table 6: The Decidability of the Set100 images using different values of radial and angular resolutions, and the best values of gabor filter parameters. Nscale=1 and it is the best for all sizes.

| Template Size	SigmaOnf	Wavelength	Decidability
8 x 256	0.5	13	4.8992
8 x 300	0.5	16	4.96
16 x 32	0.5	10	1.1278
16 x 64	0.6	10	1.7909
16 x 90	0.6	10	2.9538
16 x 128	0.6	10	4.7544
16 x 256	0.6	13	6.0943
20 x 30	0.5	10	1.1546
20 x 60	0.6	10	1.737
20 x 120	0.55	10	4.6199
20x160	0.6	10	5.7709
20 x 200	0.6	10	6.2738
20x 240	0.6	12	6.4383
24x128	0.6	10	4.8141
24 x 200	0.5	10	6.0352
32 x 32	0.55	10	1.213
32 x 64	0.6	10	2.0081
32 x 128	0.6	10	4.8698
32 x180	0.5	10	5.948

As shown in table 6, the maximum decidability will be when using template size of [20x240]. On the other hand it is noted that using template size of [20x200] also gives good decidability and there is no big difference between it and using [20x240], therefore, it is recommend using the template resolution of [20x200] to reduce the template size and consequently makes the encoding process more efficient.

5.8 Number of Shifts

Various numbers of shifts are tested to find the optimal number of shifts for iris recognition. The intra-class hamming distance distribution is analyzed when increasing the number of shifts. As shown in the experiments, the rotational inconsistencies were decreasing, the mean and the standard deviation were converging to a constant value. Figures 19 and 20 show the experiments results on various numbers of shifts.
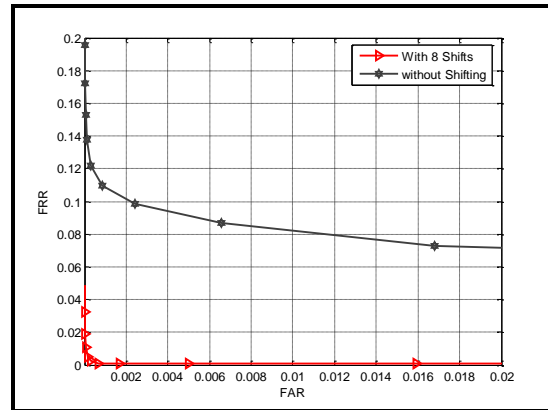
Figure 19. Roc Curve of the system when using 8 shifts and without shifts, using Set2421 and applying the optimal values of the parameters
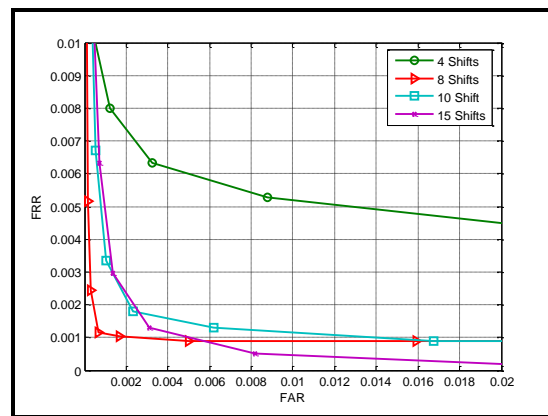

Figure 20. The ROC curves of a different number of shifts, using Set2421 and applying the optimal values of the parameters

5.9 Decidability versus Number of Images

To study the effect of changing the sample size on the decidability four datasets are chosen from the CASIAv3-Interval dataset. Images were selected serially, the number of images in each dataset and intra-class and inter-class comparisons are shown in the table 7 and figure 21.

Table 7: Intra-class and inter-class comparisons of the datasets

| Dataset	Number Of Images	No. of intra-class comparisons	No. of inter-class comparisons
Set100	100	450	4500
Set800	800	2777	316823
Set1600	1600	5166	1274034
Set2421	2421	7756	2921654
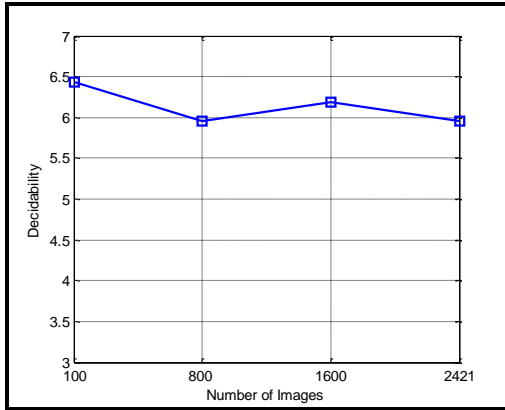
Figure 21. The decidability versus the number of images

The optimal values the gabor filter parameters that give the maximum decidability for each dataset and false accept and false reject error rates are represented in table 8 and figure 22.

Table 8. The maximum decidability and optimal values of filter parameters for each dataset. For all datasets the optimal value of Nscales=1.

Dataset	Wavelength	SigmaOnf	Decidability	FRR	FAR	HD Threshold
Set100	12	0.6	6.4383	0%	0%	0.39
Set800	12	0.45	5.9088	0.25%	0.14%	0.4
Set1600	13	0.5	6.1927	0.14%	0.08%	0.4
Set2421	12	0.45	5.9567	0.12%	0.07%	0.4
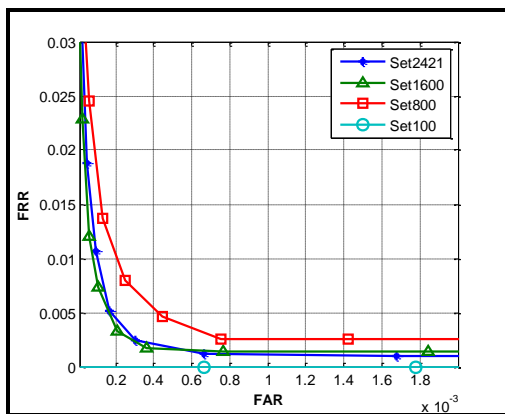
Figure 22. Comparisons between ROC curves of different number of image

As shown in table 8 and figures 21 and 22, the decidability and the error rates change between different numbers of images. This may refer to reasons such as the quality of the images, and the correctness of the segmentation especially with eyelids and eyelashes.

6. Conclusion

All evaluation experiments are done using new version of well-known database CASIA-IrisV3. Two subsets images are taken from CASIAv3-Interval, the first is Set100 contains 100 images and the second is Set2421 that contains 2421 images. The success rate of the CASIAv3-Interval images segmentation is 91.2%, some images are failed in the segmentation due to its poor quality.

The uniqueness of the iris patterns is verified by examining the Inter-Class distribution and the DOF, and the achieved DOF are 1338 for the Set100 and 1122 for the Set2421, which indicates the uniqueness of the irises patterns. The optimum values that give the maximum decidability is recorded, for Set100 they are 0.6, 12, 1 of SigmaOnf,Wavelength and number of filters respectively. For Set2421 they are 0.45, 12, 1 of SigmaOnf, Wavelength and number of filters respectively. FAR and FRR with separation point 0.4 using Set2421 are 0.12% and 0.07% respectively. The template size that gives the maximum decidability values is [20X240],but we recommend using template of size[20x200] to reduce the size, especially that there is no big difference in decidability between them, and the recommended number of shifts that are used to compensate the rotational inconsistencies is eight .

The experiments that are done using data sets contain different number of images indicate that changes in the decidability, and the error rates, FRR and FAR, may depend on images quality and the correctness of segmentation.

One of the future works we intend to reduce the system error rates by improving the segmentation to hold the images with low qualities. and applying the modified 2-LOG-Gabor filter algorithm in the encoding stage proposed by Yao et al. (Yao et al, 2006) instead of using 1-D Log, they claimed that more robust system performance can be achieved.

Acknowledgments

References

1. CASIA, (2003), Chinese Academy of Sciences – Institute of Automation. Database of 756 Greyscale Eye Images, Version 1.0. http://www.sinobiometrics.com.
2. CASIA-IrisV3, Chinese Academy of Sciences – Institute of Automation http://www.cbsr.ia.ac.cn/IrisDatabase

3. CASIA,(2006),Chinese Academy of Sciences, "Note on CASIAirisv3". http://www.cbsr.ia.ac.cn/IrisDatabase.htm.

4. Daugman J. (1993). "Confidence Visual Recognition of Persons by a Test of Statistical Independence". IEEE Transactions on Pattern Analysis and Machine Intelligence, Vol.15(11), pp.1148–1161.

5. M.S.M. Rahim, A. Rehman, Ni'matus S., F. Kurniawan and T. Saba (2012) Region-based Features Extraction in Ear Biometrics, International Journal of Academic Research, vol. 4(1), pp.37-42.

6. Daugman. J., (2003). "Demodulation by Complex-Valued Wavelets for Stochastic Pattern Recognition". International Journal of Wavelets, Multiresolution and Information Processing, Vol.1 (1), pp.1–17.

7. Daugman J., (2004)."How Iris Recognition Works", IEEE Transactions on. Circuits and Systems for Video Technology vol. 14. Pp21-30.

8. Duda O. and Hart P. (1972). "Use of the Hough Transform to Detect Lines and Curves in Pictures," CACM, Vol. 15, Jan. pp. 11-15.

9. Jain A. K., Ross A., and Prabhakar S., (2004). " An Introduction to Biometric Recognition", IEEE Transactions on Circuits and Systems for Video Technology, Special Issue on Image and Video-Based Biometrics, Vol. 14, No. 1, pp. 4-20

10. Jain, A.K., Bolle, R. and Pankanti, S., Editors, (1999). "Biometrics: Personal Identification in Networked Society", Kluwer Academic Publishers.

11. Jonathon P., Bowyer W., Flynn P.(2007), " Comments on the CASIA version 1.0 Iris Data Set", Pattern Analysis and Machine Intelligence, IEEE Transactions on Volume 29, Issue 10.pp.1869 – 1870.

12. Kovesi P. (2001) "What Are Log-Gabor Filters and Why Are They Good", Retrieved December 22, 2007, from http://www.csse.uwa.edu.au/~pk/Research/MatlabFns/ PhaseCongruency/Docs/convexpl.html.

13. Liu X., Bowyer K, and Flynn P., (2005)."Experimental Evaluation of Iris Recognition", IEEE Computer Society Conference On Computer Vision And Pattern Recognition (CVPR'05).

14. Elarbi-Boudihir, M. A. Rehman and T.Saba (2011). "Video Motion Perception Using Operation Gabor Filter". International Journal of Physical Sciences, Vol. 6(12), pp. 2799-2806.

15. Masek L., and Kovesi P., MATLAB Source Code for a Biometric Identification System Based on Iris Patterns. The School of Computer Science and Software Engineering, The University of Western Australia. 2003.

16. Saba T, Al-Zaharani S, Rehman A. (2012) Expert System for Offline Clinical Guidelines and Treatment Life Sci Journal; vol. 9(4):2639-2658.

17. Rehman, A. and Saba, T. (2013) An intelligent model for visual scene analysis and compression. Int. Arab J. Inf. Technol. Vol. 10(2): pp.126-136.

18. Wildes R., (1997). "Iris recognition: an emerging biometric technology". Proceedings of the IEEE, Vol. 85, No. 9

19. Yao P., Li J., Zhuang Z., and Li B. (2006). "Iris Recognition algorithm Using Modified Log-Gabor Filters". Proceeding of the 18th International Conference on Patterns Recognition (ICPR'06).

20. Saba, T. Altameem, A. (2013) Analysis of vision based systems to detect real time goal events in soccer videos, Applied Artificial Intelligence 27(7), 656-667

7/28/2013